THE JOURNAL OF PHYSICAL CHEMISTRY Letters

Letter

Cite This: J. Phys. Chem. Lett. 2018, 9, 588–595

pubs.acs.org/JPCL

Maximal Predictability Approach for Identifying the Right Descriptors for Electrocatalytic Reactions

Dilip Krishnamurthy,[†,§] Vaidish Sumaria,[‡,§] and Venkatasubramanian Viswanathan*[,†,‡]

[†]Department of Mechanical Engineering and [‡]Department of Chemical Engineering, Carnegie Mellon University, Pittsburgh, Pennsylvania 15213, United States

Supporting Information

ABSTRACT: Density functional theory (DFT) calculations are being routinely used to identify new material candidates that approach activity near fundamental limits imposed by thermodynamics or scaling relations. DFT calculations are associated with inherent uncertainty, which limits the ability to delineate materials (distinguishability) that possess high activity. Development of error-estimation capabilities in DFT has enabled uncertainty propagation through activity-prediction models. In this work, we demonstrate an approach to propagating uncertainty through thermodynamic activity models leading to a probability distribution of the computed activity and thereby its expectation value. A new metric, prediction efficiency, is defined, which provides a quantitative measure of the ability to distinguish activity of materials and can be used to identify the optimal descriptor(s) ΔG_{opt}. We demonstrate the framework for four important electrochemical reactions: hydrogen evolution, chlorine evolution, oxygen reduction and oxygen evolution. Future studies could utilize expected activity and prediction efficiency to significantly improve the prediction accuracy of highly active material candidates.

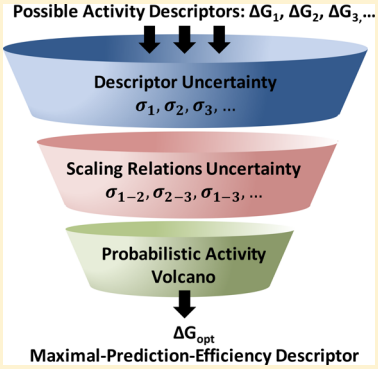

High-throughput material screening in heterogeneous electrocatalysis has been enabled by advances in density functional theory simulations.[1] Electrocatalysis has seen numerous success stories for theory-guided material design through the use of descriptor-based searchers in hydrogen evolution,[2−4] oxygen reduction,[5,6] hydrogen peroxide synthesis[7−9] and oxygen evolution.[10,11] Often, the existence of scaling relations allows multiple descriptor choices, for e.g., adsorption free energy of O*[12] or OH*[6,13] for the oxygen reduction reaction (ORR). Given the importance of the activity descriptor(s), which are currently determined based on a mechanistic understanding, a quantitative theoretical basis for the selection of descriptors is necessary. In parallel, an emergent frontier in DFT is the incorporation of uncertainty associated with predictions. The development of Bayesian error estimation functional (BEEF) has brought error-estimation capabilities to DFT simulations by generating an ensemble of functionals to map known uncertainties in the training data sets of the XC functionals.[14] In this work, we incorporate uncertainty by treating the descriptor as a probabilistic variable, which allows us to compute the probability density function (PDF) of the activity through the corresponding activity-prediction model. Based on the expectation value of the activity, we define prediction efficiency to quantify the ability of a given choice of descriptor to distinguish highly active material candidates. We use prediction efficiency to choose the ΔG_{opt} for (i) hydrogen evolution reaction, (ii) chlorine evolution reaction, (iii) oxygen reduction reaction ($2e^-$ and $4e^-$) and (iv) oxygen evolution reaction.

Let us consider the descriptor to be a normal distribution, $X \sim \mathcal{N}(\mu, \sigma^2)$, with the standard Gaussian probability density function, $p_x(x \mid \mu,\sigma^2)$, and we will revisit this assumption in the next section. The activity, now a probabilistic quantity, is given by $A = f(X)$. The associated PDF, $\hat{p}_a(a)$ can be written as $\hat{p}_a(a) = \int_{-\infty}^{+\infty} p_x(x)\delta(f(x) - a)\, dx$. The normalized PDF, $p_a(a)$, can be obtained subsequently, and the expectation value of the activity can be obtained as the probability density weighted average. $E[A] = \int_{a_{min}}^{a_{max}} a p_a(a)\, da$. In order to build intuition about the properties of the expected activity, we prove the following:

Theorem 1: *As $\sigma \to 0$ for the descriptor PDF, the expected value of the activity, $E[A] \to f(\mu)$.* Given $\sigma \to 0$, it implies that $p(x) = \delta(x-\mu)$.

$$\Rightarrow p(a) = \int_{-\infty}^{+\infty} \delta(x - \mu)\delta(f(x) - a)\, dx = \delta(f(\mu) - a)$$

$$\Rightarrow E[A] = \int_{a_{min}}^{a_{max}} a\delta(a - f(\mu))\, da = f(\mu)$$

$$\Rightarrow \lim_{\sigma \to 0} E[A] = f(\mu)$$

Theorem 2: *When the functional relationship between the descriptor and the activity, $A = f(X)$, is concave, $f(\mu) > E[A]$.* A concave function, $f(x)$, obeys $f(\sum \alpha_i x_i) > \sum(\alpha_i f(x_i))$ for $\sum \alpha_i = 1$. Choosing α_i such that $\alpha_i = p_x(x)$,

Received: October 31, 2017
Accepted: January 9, 2018
Published: January 10, 2018

DOI: 10.1021/acs.jpclett.7b02895
J. Phys. Chem. Lett. 2018, 9, 588–595

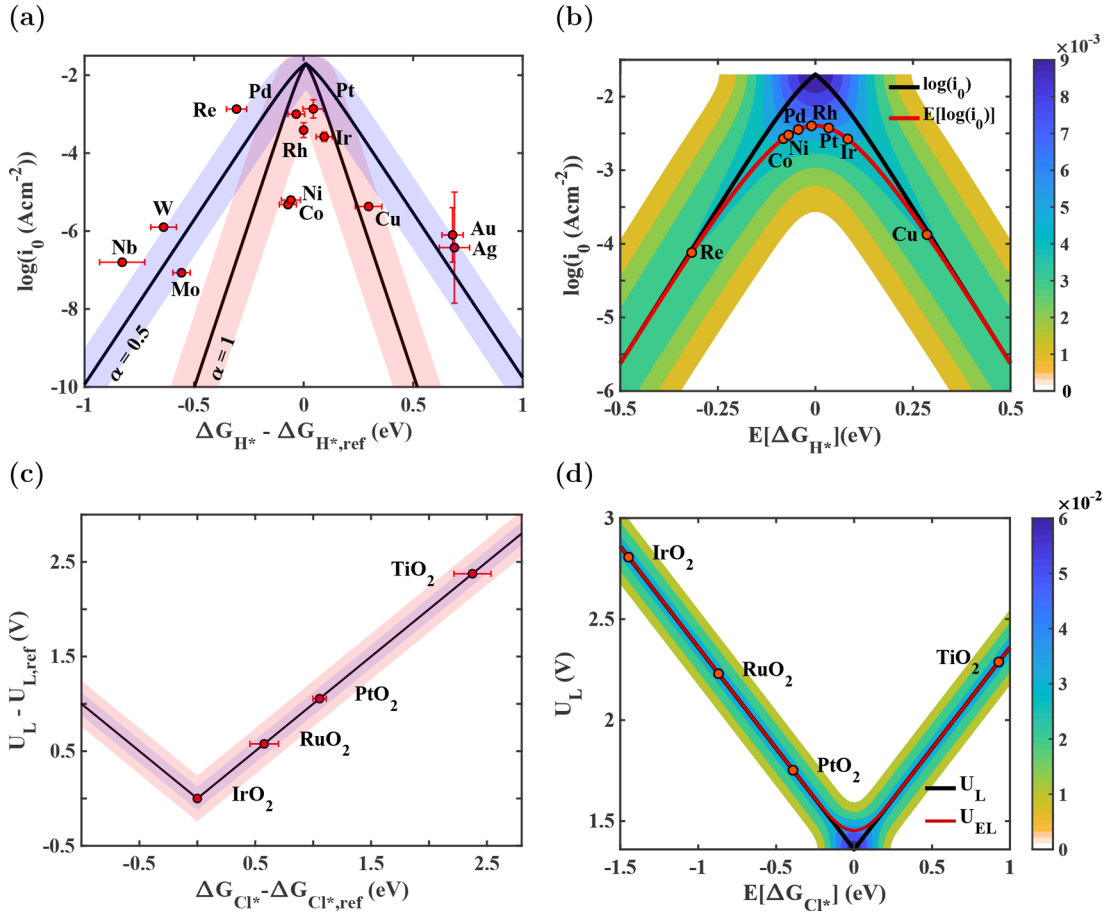

Figure 1. (a) Exchange current density prediction with one standard deviation (shaded regions) from the kinetic model (black) based on the computed hydrogen binding energy (referenced to rhodium) and the experimentally measured activity (red dots) as compiled by Nørskov et al.[4] (b) Probability map of the activity as a function of the expectation value of the hydrogen adsorption energy computed using the outlined probabilistic uncertainty propagation framework outlined. The red line represents the expected activity, depicting reduced distinguishability of materials along the activity axis. The area between the red and black lines represents the region of computational uncertainty, implying that finding candidates in this region (highly active candidates) requires higher-order computation coupled with experiments. (c) Limiting potential as a function of the free energy of chlorine adsorption referenced to IrO_2 to minimize systematic errors in DFT. The solid line represents the predicted value from the volcano relationship, whereas the colored regions represent uncertainty (1-σ and 2-σ regions). (d) Probability distribution of the limiting potential plotted versus the expectation value of the free energy of chlorine adsorption.

$$\Rightarrow f(\sum p_i x_i) > \sum (p_i f(x_i))$$

since, by definition,

$$\sum p_i x_i = \mu \text{ and } \sum (p_i f(x_i)) = E[A]$$

$$\Rightarrow f(\mu) > E[A]$$

Theorem 3: *At the maximal functional value,* a_{max}, $E[A] < a_{max}$ $\forall$ $f(X)$. By definition, $f(x) < a_{max}$ $\forall$ x. Multiplying by a positive quantity, $p_x(x_i)$, on both sides,

$$\Rightarrow p_x(x_i) f(x_i) < p_x(x_i) a_{max}$$

Now, summing this up for all i,

$$\Rightarrow \sum p_x(x_i) f(x_i) < \sum p_x(x_i) a_{max}$$

Since a_{max} does not depend on i, $\Rightarrow E[A] < a_{max}$.

In order to utilize these theorems, the descriptor PDF needs to be determined, which is enabled by the recent development of the BEEF to the XC functionals.[14] We demonstrate the use of error-estimation capabilities within the BEEF-vdW XC functional for obtaining the PDFs of descriptors through an ensemble of functionals. This approach has been utilized to quantify the uncertainty associated with reaction energies,[15,16] mechanical properties,[17] and magnetic ground states.[18] The details of the performed DFT computation are included in the Supporting Information. With the descriptor PDF determined, a key question that arises is how the predictability with the associated uncertainty compares to the case with no uncertainty, which we term as oracle (perfect) computation. Distinguishability can be understood as the ability to delineate the activity difference of different materials. Typically, in electrocatalysis, we are interested in identifying materials that possess a certain threshold activity, which in computational electrocatalysis is typically the threshold limiting potential, U_T. This leads to a finite interval of the descriptor values of interest. For this range of descriptor values, the activity with perfect computation (no uncertainty) in the descriptor space maps to an interval $[U_T, \max(U_L)]$, while that with uncertainty in the descriptor maps to $[U_T, \max(U_{EL})]$, where U_{EL} is the expectation value of the limiting potential. An obvious approach to delineate materials is directly quantified by the length of this interval. A mathematically precise definition of the ability to distinguish materials is the Lebesgue measure of the interval,

DOI: 10.1021/acs.jpclett.7b02895
J. Phys. Chem. Lett. 2018, 9, 588−595

which can be used readily for predicting more than one property of interest. Based on this, we define prediction efficiency to be a quantity given by the ratio of the distinguishability with uncertainty to the distinguishability with perfect computation, i.e., oracle computation. The prediction efficiency is expressed as

$$\eta_{\text{pred}}(U_{\text{T}}) = \frac{\lambda([U_{\text{T}}, \max(U_{\text{EL}})])}{\lambda([U_{\text{T}}, \max(U_{\text{L}})])}$$

where, λ is the Lebesgue measure of the interval, which is its length in one-dimension. We can build intuition on prediction efficiency based on the following properties. With this definition, as $\sigma \to 0$ for the descriptor PDF, the prediction efficiency $\eta_{\text{pred}} \to 1$. If f is concave, based on Theorem 2, the prediction efficiency, $\eta_{\text{pred}} < 1$ for $\sigma \neq 0$. As we will show later, the prediction efficiency can be used to (i) quantify the efficiency of a particular descriptor for an electrocatalytic reaction scheme, and (ii) quantitatively compare predictability between different electrochemical reactions.

The probabilistic approach is first illustrated for hydrogen evolution reaction owing to a unique atomic-scale descriptor for its catalytic activity.[19] The HER has gained renewed interest in solar water-splitting for hydrogen production,[20,21] requiring computational-screening approaches for identifying active catalysts. For prediction of HER activity before DFT-enabled computations, Parsons identified through a mechanistic understanding that the descriptor is the free energy of hydrogen adsorption.[19] However, due to the then calorimetric limitations, for decades the descriptor was approximated to be the metal-hydride bond strength.[19] With the development of DFT, it has been made possible to compute the hydrogen binding energy (ΔG_{H^*}) in agreement with experimental measurements, which has been used in numerous successful screening approaches.[2−4] In this work, we use this descriptor to demonstrate our probabilistic formalism for activity prediction by following the Volmer−Heyrovsky reaction mechanism.[22] In this mechanism, the first step is the activation of protons as adsorbed hydrogen, and a subsequent step is a concerted proton−electron addition to evolve hydrogen. The descriptor, the hydrogen binding energy, and the activity can be linked through a simplified kinetic model[4] as

$$i_0 = f(\Delta G_{\text{H}^*}) = -ek_0(1 + \exp(|\Delta G_{\text{H}^*}|/kT))^{-1}$$

where the pre-exponential factor is obtained by fitting to experiments. To demonstrate the probabilistic approach, we consider a range of transition metals that are known to be active hydrogen-evolution catalysts and the predicted exchange current density is shown in Figure 1a. Within our uncertainty-propagation framework, as presented in an earlier work we approximate the descriptor uncertainty to be uniform and is given by the standard deviation of the combined distribution of the descriptor, σ_H, from all the metals.[13] We treat the descriptor as a Gaussian probabilistic variable, $X \sim \mathcal{N}(\mu, \sigma_{\text{H}}^2)$, with an associated PDF, $p_x(x|\mu,\sigma_{\text{H}}^2)$. To propagate the descriptor uncertainty, we map this PDF through the kinetic model onto the exchange current density axis, and the activity PDF can be expressed as

$$\hat{p}_{i_0}(i_0) = \int_{-\infty}^{+\infty} p_x(x)\delta(f(x) - i_0)\, \mathrm{d}x$$

which is normalized to obtain $p_{i_0}(i_0)$, the activity PDF. Figure 1b shows the PDF map of the activity as a function of μ, the mean value of the descriptor PDF. From the activity PDF, the expectation value of activity is obtained using the normalized PDF $p\,(i_0)$ as

$$i_{0E} = \int_{-\infty}^{i_{0_{\max}}} i_0 p_{i_0}(i_0)\, \mathrm{d}i_0$$

The red curve in Figure 1b represents the expected-activity curve and the distinguishability of activity between candidates is the lowest near the top of the volcano. This implies that through a purely computational approach, with the current DFT accuracy, the predicted activity of candidates like Pt, Pd, and Rh are indistinguishable. Therefore, efforts with a quest to identify catalysts in acidic media better than the archetypical HER catalyst, platinum, must be cautiously designed within purely computationally driven approaches.

We extend the framework to the chlorine evolution reaction (ClER), which is one of the largest technological applications of electrochemistry. It occurs as a two-electron process through a few possible pathways with a well-studied descriptor for its catalytic activity. While the ClER is a hugely important reaction, the search for effective catalysts has largely been driven by empiricism. Through an empirical approach, the development of Dimensionally Stable Anodes by Beer[23] forms a milestone for the chlor-alkali industry demonstrating a synergistic enhancement of stability and activity over a broad range of operating conditions.[24] The mechanistic understanding of the ClER was largely driven by experimental work by Krishtalik et al.[25] However, oxygen evolution tends to occur as a parasitic reaction, especially at high current densities, since the equilibrium potentials for chlorine evolution and oxygen evolution are close and rutile oxides catalyze both reactions.[26] Undoubtedly, the possible competing pathways affect the specific activity, however, we adopt a simplistic mechanism to demonstrate our probabilistic framework by following the Volmer−Heryrovski mechanism. Since the mechanism involves a single intermediate, the chlorine adsorption energy forms the descriptor for activity and it is possible to attain the equilibrium potential. The limiting potential can be determined[26] as $U_{\text{L}} = f(\Delta G_{\text{Cl}^*}) = 1.36 + |\Delta G_{\text{Cl}^*}|$ V. We consider rutile oxides, which are reported to be active chlorine-evolution catalysts (Figure 1c). We follow a similar approach to that demonstrated for HER, to propagate the descriptor uncertainty (σ_{Cl}) to the activity (Figure 1d), where the red curve represents the expected activity. The distinguishability of activity between candidates with descriptor values near the apex of the volcano is the lowest, as implied in theorem 2. The reduced distinguishability can be attributed solely to the descriptor uncertainty since there exists only a single intermediate (descriptor), which also results in a high prediction efficiency for ClER relative to reactions with multiple descriptor choices, as we demonstrate later (Figure 4). We observe from the prediction efficiency curve that for overpotentials below 0.9 V, the prediction efficiency is zero, implying that higher-order DFT methods are necessary for screening approaches to identify candidate catalysts with very low overpotentials.

The fundamental understanding of the ORR has largely been through the surface science approach to electrocatalysis,[27−36] which relies on surface analytical tools[33,36−40] complemented by first-principles calculations.[12,41−46] For computational screening, multiple choices of the descriptor for ORR activity

DOI: 10.1021/acs.jpclett.7b02895
J. Phys. Chem. Lett. 2018, 9, 588−595

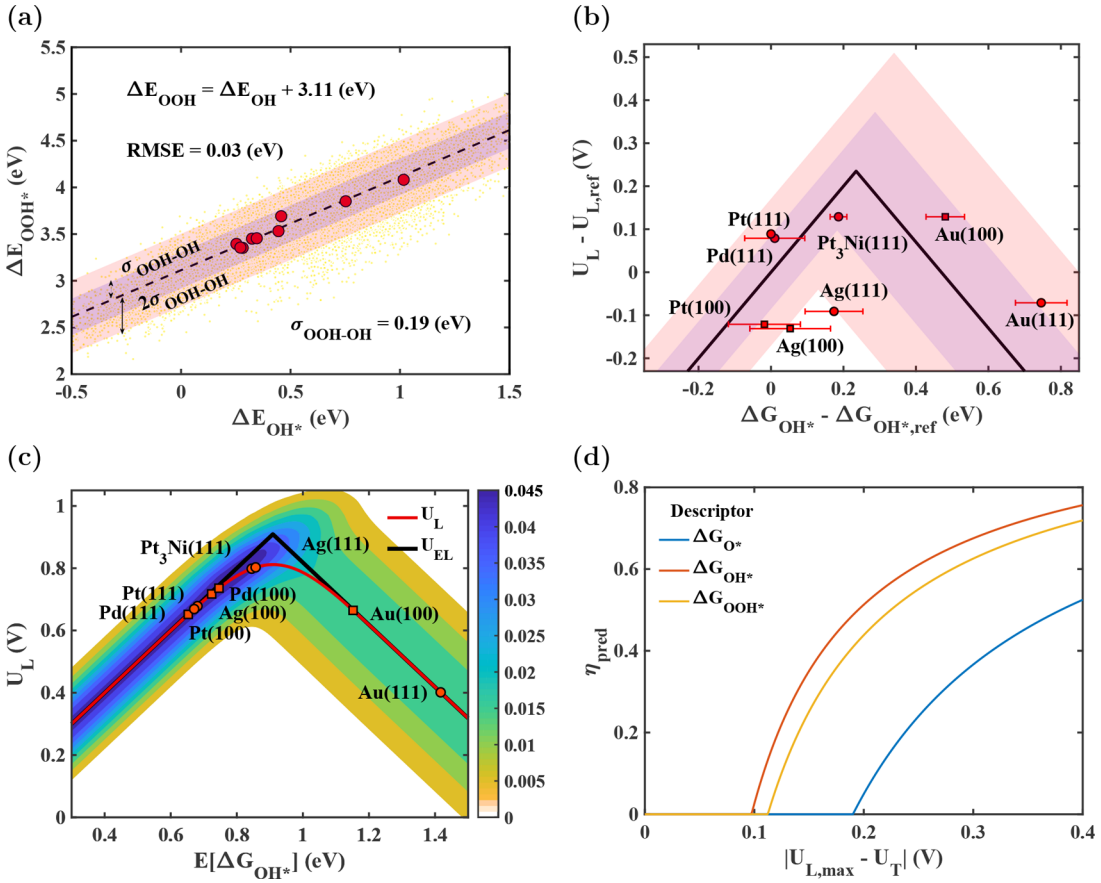

Figure 2. (a) Computed scaling relation between adsorption energies of the intermediates, OH* and OOH*. The red dots represent DFT-calculated free energies, and the yellow dots represent those computed from the family of functionals within BEEF-vdW, enabling error estimation. The two shaded regions represent one and two standard deviations in the scaling intercept. Similar scaling is found between the adsorption energies of other oxygen intermediates (shown in the Supporting Information). (b) Activity volcano for 4e$^-$ ORR showing the experimentally measured limiting potentials plotted against the DFT-calculated adsorption free energy of OH* relative to Pt(111). (c) Probabilistic activity volcano using ΔG_{OH*}, which we identify as the descriptor that maximizes the prediction efficiency. (d) Prediction efficiency as a function of the activity interval of interest, $|U_{L,max} - U_T|$. It can be seen that ΔG_{OH*} is the descriptor that maximizes predictability for 4e$^-$ ORR.

have been used based on free energy scaling between intermediates.[13,47] Greeley et al. showed that specific Pt-based binary alloys exceed the activity of Pt by using the free energy of adsorbed oxygen as the descriptor.[47] By contrast, Ifan et al. identified Pt_5La to have significantly higher activity than Pt by using the free energy of OH* as the descriptor.[48] A rational approach to choosing the right descriptor for the ORR is not present and in this work, we fill this gap with conclusions, similar to that shown in an earlier work.[13]

We follow the associative mechanism for the 4e$^-$ reduction,[12] and the electrocatalytic activity for ORR is determined by the free energies of adsorbed OOH*, OH* and O*. However, the presence of scaling[49] between these intermediates allows us to use a single descriptor for the activity.[10,48,50] We apply the probabilistic approach by considering various metallic facets and propagate the uncertainty in the descriptor and scaling relations to predict ORR activity. Scaling relations between the adsorbates (Figure 2a and Figure S6) allow us to describe the limiting potential as a function of one descriptor (Figure 2b). The slopes of the scaling relations have been fixed in accordance with bond-order conservation principles and the intercept uncertainty is obtained using Bayesian error estimation within the BEEF-vdW XC functional. Let us begin with the case of the free energy of OH*, G_{OH*}, being the descriptor, where the limiting potential is given by $U_L = f(\Delta G_{OH*}) = \min(\Delta G_{OH*}, 4.92 - \Delta G_{OOH*})$. Hence, using the scaling relations, the limiting potential is expressed as $U_L = \min(\Delta G_{OH*}, 4.92 - (3.11 + \Delta G_{OH*}))$ V. The descriptor uncertainty is approximated based on the combined distribution of the surfaces explored.[13] The uncertainty in the scaling relation is incorporated by considering an ensemble of activity volcano relationships mapped from the ensemble of scaling relation intercepts. For each member of the ensemble of volcano relationships, the descriptor uncertainty is propagated. This allows us to compute the expected activity for each ensemble member and a probability-weighted average gives the activity PDF and the expected limiting potential (Figure 2c). In a similar manner, we construct the PDF maps of ORR activity and the corresponding expected limiting potentials using ΔG_{OH*} and ΔG_{O*} as the descriptors (Figure 2d,e). For the three descriptors, we can compare the predictability of activity based on the prediction efficiency. We find that the prediction efficiency follows the trend, $\eta_{pred}^{OH*} > \eta_{pred}^{OOH*} > \eta_{pred}^{O*}$, identifying that ΔG_{OH*} is the descriptor for maximal predictability. It is worth highlighting that the use of ΔG_{O*} as the descriptor uses two scaling relations, while ΔG_{OH*} and ΔG_{OOH*} use only one, leading to improved prediction efficiency. We demonstrate the ΔG_{opt} choice through a similar approach for 2e$^-$ oxygen reduction in the Supporting Information (section 5.5).

DOI: 10.1021/acs.jpclett.7b02895
J. Phys. Chem. Lett. 2018, 9, 588−595

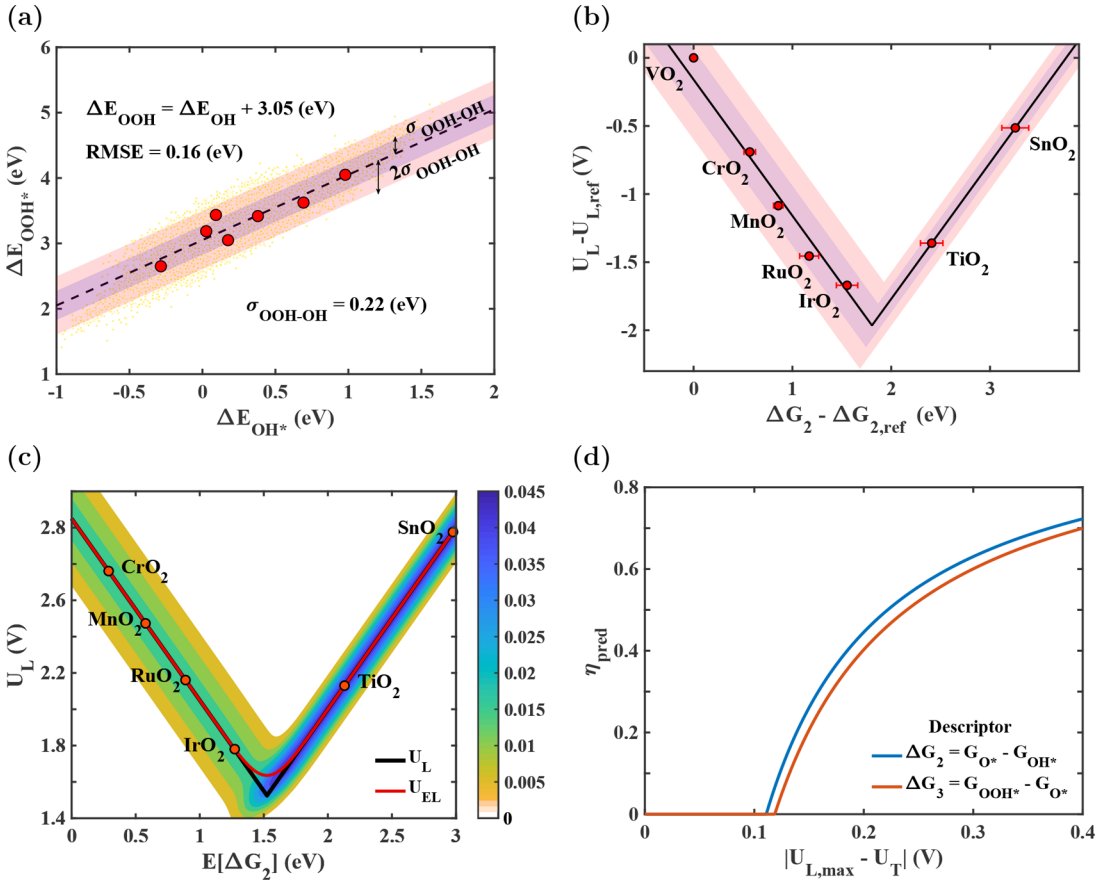

Figure 3. (a) The computed scaling relation between the binding energies of the intermediates, OH* and OOH*, with the associated uncertainty in the intercept. (b) The limiting potential as a function of the descriptor. $\Delta G_2 = G_{O^*} - G_{OH^*}$. The shaded regions represent the uncertainty and the error-bars convey the descriptor uncertainty referenced to VO_2. (c) Probability map of the limiting potential as a function of the expectation value of the descriptor ($E[\Delta G_2]$). The red curve represents the predicted expected activity, U_{EL}. (d) Comparison of the prediction efficiencies of the two descriptors. Among the two, ΔG_2 provides higher distinguishability of materials, by enhancing the prediction efficiency for oxygen evolution.

We show the effectiveness of the probabilistic approach by also extending to the oxygen evolution reaction (OER), which is carried out under harsh oxidizing conditions and is a crucial process for the solar fuel generation.[20] The foundational understanding of the OER on metal oxides has been built largely through experimental measurements and by empirically correlating them to the enthalpy of lower to higher oxide transition.[24,51] The insights developed using this approach have been limited due to the inability to accurately measure chemisorption energies. This is due to the difficulty associated with preparing well-ordered single-crystalline oxides and the limited electrical conductivity, making them challenging for surface characterization.[52]

On the theoretical front, progress in understanding electrocatalysis has been limited by the accuracy of DFT in describing correlation in transition metal oxides.[53,54] Using appropriate reference schemes, it has been shown that the formation energies of rutile oxides can be described well using DFT at the GGA level.[55] Man et al. explored trends in reactivity for oxygen evolution on rutile and perovskite surfaces, showing the existence of scaling relations.[10] Based on this analysis, they argued that $\Delta G = \Delta G_{O^*} - \Delta G_{OH^*}$ can be used as a descriptor for predicting activity. Subsequently, two independent descriptors were used to predict the overpotential.[56] Despite these advances, the selection of the right descriptor for oxygen evolution remains elusive. We fill this gap by exploring the associative mechanism for oxygen evolution on rutile oxide (110) surfaces. The OER activity is determined by the adsorption energy of the reaction intermediates. We find that the scaling between the adsorption energies of OOH* and OH* has a slope close to 1 and the intercept is found to be 3.05 (Figure 3a).[10,57] The variation in the limiting-potential is therefore determined by ΔG_{O^*}. Hence, we can use $\Delta G_2 = (\Delta G_{O^*} - \Delta G_{OH^*})$ or $\Delta G_3 = (\Delta G_{OOH^*} - \Delta G_{O^*})$ as a descriptor. This implies that $U_L = \max(\Delta G_2, 3.05 - \Delta G_2) = \max(\Delta G_3, 3.05 - \Delta G_3)$. Following a similar approach to ORR, we show a probabilistic activity plot as a function of descriptors, $E[\Delta G_2]$ and $E[\Delta G_3]$, in Figures 3c and S11. We quantitatively demonstrate that ΔG_2 is the ΔG_{opt} for OER based on the prediction efficiency (Figure 3d).

The developed approach allows a quantitative comparison of the prediction efficiency across different electrochemical reactions. We show a plot of the prediction efficiency for the ΔG_{opt} as a function of the overpotential for the considered electrochemical reactions in Figure 4. Based on this analysis, we find that the prediction efficiency for $2e^-$ electrochemical reactions such as HER and ClER is greater than that for $4e^-$ ORR and OER. This suggests that the likelihood of utilizing DFT calculations to identify highly active candidates will be more probable for $2e^-$ reactions compared to $4e^-$ reactions. Further, the differences in prediction efficiency between $2e^-$ and $4e^-$ suggest that predicting selectivity trends is fraught with challenges and requires a revisiting of the utilized descriptor that aims to optimize prediction efficiency for selectivity.

DOI: 10.1021/acs.jpclett.7b02895
J. Phys. Chem. Lett. 2018, 9, 588−595

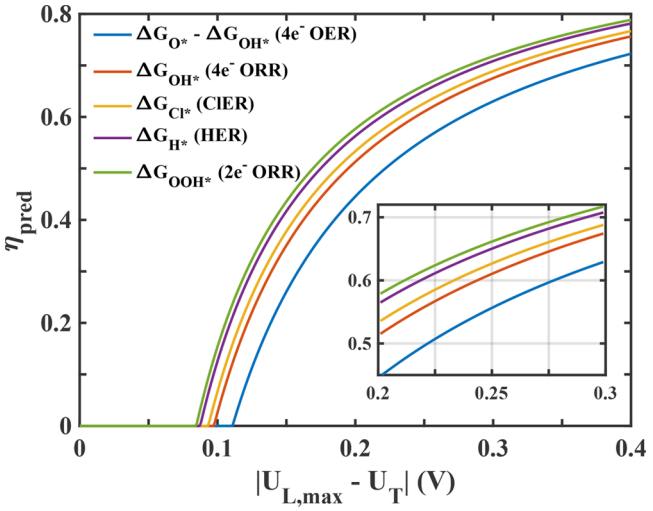

Figure 4. Prediction efficiency, η_{pred}, as a function of $|U_{L,max} - U_T|$, which represents the activity interval of interest for screening. It can be quantitatively seen that the ability of DFT to delineate materials decreases with increasing number of elementary electrochemical steps involved. Identifying highly active materials for oxygen reduction ($4e^-$) and oxygen evolution, therefore, requires screening through a synergistic approach involving experiments and theory.

In this work, although we have obtained the descriptor PDF using the BEEF-vdW XC functional, the probabilistic uncertainty-propagation framework is universally applicable regardless of the origin of the descriptor PDF. For example, the descriptor PDFs could be obtained from machine learning based models.[58] It is worth highlighting that the prediction efficiency is determined by the descriptor uncertainty (σ), which could be reduced with higher-order DFT methods. mBEEF is a meta-GGA based functional, with built-in error estimation capability.[59] This functional could give rise to lower descriptor uncertainty leading to improved prediction efficiency. We suggest two approaches without increased computational complexity, through the use of (i) hybrid material reference, and (ii) hybrid descriptors. We demonstrate in the Supporting Information that a two-material reference scheme for oxygen reduction leads to increased prediction efficiency. Specifically, we show that referencing relative to a combination of Pt and Au leads to improved prediction efficiency. Reference states leading to systematic error reduction is widely established for bulk formation energies.[55,60]

We have presented a method to carry out robust material selection through a systematic approach of incorporating uncertainty in density functional theory calculated energies. We propose that for increased prediction accuracy, screening studies should be based on the expected activity from the probabilistic approach. We define a quantity termed as the prediction efficiency, which can be used to identify the ΔG_{opt} and compare the predictability of DFT across different electrochemical reactions. The prediction limit, which is the highest expected activity, represents the activity above which no assertive prediction can be made using computational approaches alone. This implies that identifying material candidates above the prediction limit requires more accurate computations and/or experiment-theory coupling. We demonstrate this by applying it to four electrochemical reactions, namely hydrogen evolution, chlorine evolution, oxygen reduction and oxygen evolution. We argue that the descriptor must be chosen such that it maximizes the prediction efficiency over the activity range of interest. We show conclusively that the ΔG_{opt} for 4 and $2e^-$ ORR are G_{OH*} and G_{OOH*}, respectively. Similarly, for oxygen evolution reaction, the ΔG_{opt} is identified to be $\Delta G_2 = \Delta G_{O*} - \Delta G_{OH*}$. Finally, across reactions, we find that the prediction efficiency for $2e^-$ electrochemical reactions such as HER and ClER is greater than that for $4e^-$ ORR and OER. We believe that the use of prediction efficiency should be ubiquitous and should form an integral part of descriptor-based activity predictions.

■ ASSOCIATED CONTENT

Supporting Information

The Supporting Information is available free of charge on the ACS Publications website at DOI: 10.1021/acs.jpclett.7b02895.

Computational details, detailed uncertainty propagation formalism for HER, ClER, ORR ($4e^-$ and $2e^-$), and OER, and approaches to improve prediction efficiency (PDF)

■ AUTHOR INFORMATION

ORCID

Venkatasubramanian Viswanathan: 0000-0003-1060-5495

Author Contributions

[§]Equal contribution

Notes

The authors declare no competing financial interest.

■ ACKNOWLEDGMENTS

D.K. and V.V. gratefully acknowledge funding support from the National Science Foundation under award CBET-1554273. V.S. and V.V. acknowledge support from the Scott Institute for Energy Innovation at Carnegie Mellon University. The authors acknowledge Dr. Isabela C. Man for sharing structure files related to oxygen evolution and chlorine evolution.

■ REFERENCES

(1) Nørskov, J. K.; Bligaard, T.; Rossmeisl, J.; Christensen, C. H. Towards the computational design of solid catalysts. *Nat. Chem.* **2009**, *1*, 37−46.

(2) Greeley, J.; Jaramillo, T. F.; Bonde, J.; Chorkendorff, I.; Nørskov, J. K. Computational high-throughput screening of electrocatalytic materials for hydrogen evolution. *Nat. Mater.* **2006**, *5*, 909−913.

(3) Greeley, J.; Nørskov, J. K.; Kibler, L. A.; El-Aziz, A. M.; Kolb, D. M. Hydrogen evolution over bimetallic systems: Understanding the trends. *ChemPhysChem* **2006**, *7*, 1032−1035.

(4) Nørskov, J. K.; Bligaard, T.; Logadottir, A.; Kitchin, J.; Chen, J. G.; Pandelov, S.; Stimming, U. Trends in the exchange current for hydrogen evolution. *J. Electrochem. Soc.* **2005**, *152*, J23−J26.

(5) Greeley, J.; Nørskov, J. K. Combinatorial density functional theory-based screening of surface alloys for the oxygen reduction reaction. *J. Phys. Chem. C* **2009**, *113*, 4932−4939.

(6) Viswanathan, V.; Hansen, H. A.; Rossmeisl, J.; Nørskov, J. K. Universality in oxygen reduction electrocatalysis on metal surfaces. *ACS Catal.* **2012**, *2*, 1654−1660.

(7) Rankin, R. B.; Greeley, J. Trends in selective hydrogen peroxide production on transition metal surfaces from first principles. *ACS Catal.* **2012**, *2*, 2664−2672.

(8) Viswanathan, V.; Hansen, H. A.; Nørskov, J. K. Selective electrochemical generation of hydrogen peroxide from water oxidation. *J. Phys. Chem. Lett.* **2015**, *6*, 4224−4228.

(9) Verdaguer-Casadevall, A.; Deiana, D.; Karamad, M.; Siahrostami, S.; Malacrida, P.; Hansen, T. W.; Rossmeisl, J.; Chorkendorff, I.; Stephens, I. E. Trends in the electrochemical synthesis of H_2O_2:

DOI: 10.1021/acs.jpclett.7b02895
J. Phys. Chem. Lett. 2018, 9, 588−595

Enhancing activity and selectivity by electrocatalytic site engineering. *Nano Lett.* **2014**, *14*, 1603−1608.
(10) Man, I. C.; Su, H.-Y.; Calle-Vallejo, F.; Hansen, H. A.; Martínez, J. I.; Inoglu, N. G.; Kitchin, J.; Jaramillo, T. F.; Nørskov, J. K.; Rossmeisl, J. Universality in oxygen evolution electrocatalysis on oxide surfaces. *ChemCatChem* **2011**, *3*, 1159−1165.
(11) Halck, N. B.; Petrykin, V.; Krtil, P.; Rossmeisl, J. Beyond the volcano limitations in electrocatalysis−oxygen evolution reaction. *Phys. Chem. Chem. Phys.* **2014**, *16*, 13682−13688.
(12) Nørskov, J. K.; Rossmeisl, J.; Logadottir, A.; Lindqvist, L.; Kitchin, J. R.; Bligaard, T.; Jonsson, H. Origin of the overpotential for oxygen reduction at a fuel-cell cathode. *J. Phys. Chem. B* **2004**, *108*, 17886−17892.
(13) Deshpande, S.; Kitchin, J. R.; Viswanathan, V. Quantifying Uncertainty in Activity Volcano Relationships for Oxygen Reduction Reaction. *ACS Catal.* **2016**, *6*, 5251−5259.
(14) Wellendorff, J.; Lundgaard, K. T.; Møgelhøj, A.; Petzold, V.; Landis, D. D.; Nørskov, J. K.; Bligaard, T.; Jacobsen, K. W. Density functionals for surface science: Exchange-correlation model development with Bayesian error estimation. *Phys. Rev. B: Condens. Matter Mater. Phys.* **2012**, *85*, 235149.
(15) Medford, A. J.; Wellendorff, J.; Vojvodic, A.; Studt, F.; Abild-Pedersen, F.; Jacobsen, K. W.; Bligaard, T.; Nørskov, J. K. Assessing the reliability of calculated catalytic ammonia synthesis rates. *Science* **2014**, *345*, 197−200.
(16) Christensen, R.; Hansen, H. A.; Dickens, C. F.; Nørskov, J. K.; Vegge, T. Functional Independent Scaling Relation for ORR/OER Catalysts. *J. Phys. Chem. C* **2016**, *120*, 24910−24916.
(17) Ahmad, Z.; Viswanathan, V. Quantification of uncertainty in first-principles predicted mechanical properties of solids: Application to solid ion conductors. *Phys. Rev. B: Condens. Matter Mater. Phys.* **2016**, *94*, 064105.
(18) Houchins, G.; Viswanathan, V. Quantifying confidence in density functional theory predictions of magnetic ground states. *Phys. Rev. B: Condens. Matter Mater. Phys.* **2017**, *96*, 134426.
(19) Parsons, R. The rate of electrolytic hydrogen evolution and the heat of adsorption of hydrogen. *Trans. Faraday Soc.* **1958**, *54*, 1053−1063.
(20) Lewis, N. S.; Nocera, D. G. Powering the planet: Chemical challenges in solar energy utilization. *Proc. Natl. Acad. Sci. U. S. A.* **2006**, *103*, 15729−15735.
(21) McCrory, C. C.; Jung, S.; Ferrer, I. M.; Chatman, S. M.; Peters, J. C.; Jaramillo, T. F. Benchmarking hydrogen evolving reaction and oxygen evolving reaction electrocatalysts for solar water splitting devices. *J. Am. Chem. Soc.* **2015**, *137*, 4347−4357.
(22) Bockris, J. O.; Mauser, H. The kinetics of the evolution and dissolution of hydrogen at electrodes. *Can. J. Chem.* **1959**, *37*, 475−488.
(23) Beer, H. B. Method of making an electrode having a coating containing a platinum metal oxide thereon. US Patent 4,052,271, 1977.
(24) Trasatti, S. Electrocatalysis in the anodic evolution of oxygen and chlorine. *Electrochim. Acta* **1984**, *29*, 1503−1512.
(25) Krishtalik, L. Kinetics and mechanism of anodic chlorine and oxygen evolution reactions on transition metal oxide electrodes. *Electrochim. Acta* **1981**, *26*, 329−337.
(26) Hansen, H. A.; Man, I. C.; Studt, F.; Abild-Pedersen, F.; Bligaard, T.; Rossmeisl, J. Electrochemical chlorine evolution at rutile oxide (110) surfaces. *Phys. Chem. Chem. Phys.* **2010**, *12*, 283−290.
(27) Marković, N.; Ross, P. N. Surface science studies of model fuel cell electrocatalysts. *Surf. Sci. Rep.* **2002**, *45*, 117−229.
(28) Mukerjee, S.; Srinivasan, S.; Soriaga, M. P.; McBreen, J. Role of structural and electronic properties of Pt and Pt alloys on electrocatalysis of oxygen reduction An in situ XANES and EXAFS investigation. *J. Electrochem. Soc.* **1995**, *142*, 1409−1422.
(29) Markovic, N. M.; Gasteiger, H. A.; Ross, P. N., Jr Oxygen reduction on platinum low-index single-crystal surfaces in sulfuric acid solution: rotating ring-Pt (hkl) disk studies. *J. Phys. Chem.* **1995**, *99*, 3411−3415.
(30) Zhang, J.; Vukmirovic, M. B.; Xu, Y.; Mavrikakis, M.; Adzic, R. R. Controlling the Catalytic Activity of Platinum-Monolayer Electrocatalysts for Oxygen Reduction with Different Substrates. *Angew. Chem., Int. Ed.* **2005**, *44*, 2132−2135.
(31) Zhou, W. P.; Yang, X.; Vukmirovic, M. B.; Koel, B. E.; Jiao, J.; Peng, G.; Mavrikakis, M.; Adzic, R. R. Improving Electrocatalysts for O_2 Reduction by Fine-Tuning the Pt- Support Interaction: Pt Monolayer on the Surfaces of a Pd_3Fe (111) Single-Crystal Alloy. *J. Am. Chem. Soc.* **2009**, *131*, 12755−12762.
(32) Kuzume, A.; Herrero, E.; Feliu, J. M. Oxygen reduction on stepped platinum surfaces in acidic media. *J. Electroanal. Chem.* **2007**, *599*, 333−343.
(33) Wakisaka, M.; Suzuki, H.; Mitsui, S.; Uchida, H.; Watanabe, M. Identification and quantification of oxygen species adsorbed on Pt (111) single-crystal and polycrystalline Pt electrodes by photoelectron spectroscopy. *Langmuir* **2009**, *25*, 1897−1900.
(34) Wakisaka, M.; Udagawa, Y.; Suzuki, H.; Uchida, H.; Watanabe, M. Structural effects on the surface oxidation processes at Pt single-crystal electrodes studied by X-ray photoelectron spectroscopy. *Energy Environ. Sci.* **2011**, *4*, 1662−1666.
(35) Kondo, S.; Nakamura, M.; Maki, N.; Hoshi, N. Active sites for the oxygen reduction reaction on the low and high index planes of palladium. *J. Phys. Chem. C* **2009**, *113*, 12625−12628.
(36) Stephens, I. E.; Bondarenko, A. S.; Perez-Alonso, F. J.; Calle-Vallejo, F.; Bech, L.; Johansson, T. P.; Jepsen, A. K.; Frydendal, R.; Knudsen, B. P.; Rossmeisl, J.; et al. Tuning the activity of Pt (111) for oxygen electroreduction by subsurface alloying. *J. Am. Chem. Soc.* **2011**, *133*, 5485−5491.
(37) Damjanovic, A.; Genshaw, M.; Bockris, J. The mechanism of oxygen reduction at platinum in alkaline solutions with special reference to H_2O_2. *J. Electrochem. Soc.* **1967**, *114*, 1107−1112.
(38) Fernández, J. L.; Bard, A. J. Scanning electrochemical microscopy. 47. imaging electrocatalytic activity for oxygen reduction in an acidic medium by the tip generation- substrate collection mode. *Anal. Chem.* **2003**, *75*, 2967−2974.
(39) Hoster, H.; Richter, B.; Behm, R. Catalytic influence of Pt monolayer islands on the hydrogen electrochemistry of Ru (0001) studied by ultrahigh vacuum scanning tunneling microscopy and cyclic voltammetry. *J. Phys. Chem. B* **2004**, *108*, 14780−14788.
(40) Stamenkovic, V. R.; Fowler, B.; Mun, B. S.; Wang, G.; Ross, P. N.; Lucas, C. A.; Markovic, N. M. Improved Oxygen Reduction Activity on $Pt_3Ni(111)$ via Increased Surface Site Availability. *Science* **2007**, *315*, 493−497.
(41) Anderson, A. B. O_2 reduction and CO oxidation at the Pt-electrolyte interface. The role of H_2O and OH adsorption bond strengths. *Electrochim. Acta* **2002**, *47*, 3759−3763.
(42) Viswanathan, V.; Hansen, H. A.; Rossmeisl, J.; Jaramillo, T. F.; Pitsch, H.; Nørskov, J. K. Simulating linear sweep voltammetry from first-principles: application to electrochemical oxidation of water on Pt (111) and Pt_3 Ni(111). *J. Phys. Chem. C* **2012**, *116*, 4698−4704.
(43) Gohda, Y.; Schnur, S.; Groß, A. Influence of water on elementary reaction steps in electrocatalysis. *Faraday Discuss.* **2009**, *140*, 233−244.
(44) Janik, M. J.; Taylor, C. D.; Neurock, M. First-principles analysis of the initial electroreduction steps of oxygen over Pt (111). *J. Electrochem. Soc.* **2009**, *156*, B126−B135.
(45) Anderson, A. B.; Uddin, J.; Jinnouchi, R. Solvation and Zero-Point-Energy Effects on OH (ads) Reduction on Pt (111). *J. Phys. Chem. C* **2010**, *114*, 14946−14952.
(46) Jinnouchi, R.; Hatanaka, T.; Morimoto, Y.; Osawa, M. First principles study of sulfuric acid anion adsorption on a Pt (111) electrode. *Phys. Chem. Chem. Phys.* **2012**, *14*, 3208−3218.
(47) Greeley, J.; Stephens, I.; Bondarenko, A.; Johansson, T. P.; Hansen, H. A.; Jaramillo, T.; Rossmeisl, J.; Chorkendorff, I.; Nørskov, J. K. Alloys of platinum and early transition metals as oxygen reduction electrocatalysts. *Nat. Chem.* **2009**, *1*, 552−556.
(48) Stephens, I. E.; Bondarenko, A. S.; Grønbjerg, U.; Rossmeisl, J.; Chorkendorff, I. Understanding the electrocatalysis of oxygen

DOI: 10.1021/acs.jpclett.7b02895
J. Phys. Chem. Lett. 2018, 9, 588−595

reduction on platinum and its alloys. *Energy Environ. Sci.* **2012**, *5*, 6744−6762.
(49) Abild-Pedersen, F.; Greeley, J.; Studt, F.; Rossmeisl, J.; Munter, T.; Moses, P. G.; Skulason, E.; Bligaard, T.; Nørskov, J. K. Scaling properties of adsorption energies for hydrogen-containing molecules on transition-metal surfaces. *Phys. Rev. Lett.* **2007**, *99*, 016105.
(50) Calle-Vallejo, F.; Koper, M. T. First-principles computational electrochemistry: Achievements and challenges. *Electrochim. Acta* **2012**, *84*, 3−11.
(51) Trasatti, S. Electrocatalysis by oxides—attempt at a unifying approach. *J. Electroanal. Chem. Interfacial Electrochem.* **1980**, *111*, 125−131.
(52) Campbell, C. T.; Sellers, J. R. Enthalpies and entropies of adsorption on well-defined oxide surfaces: Experimental measurements. *Chem. Rev.* **2013**, *113*, 4106−4135.
(53) Cohen, A. J.; Mori-Sánchez, P.; Yang, W. Insights into current limitations of density functional theory. *Science* **2008**, *321*, 792−794.
(54) Wang, L.; Maxisch, T.; Ceder, G. Oxidation energies of transition metal oxides within the GGA+ U framework. *Phys. Rev. B: Condens. Matter Mater. Phys.* **2006**, *73*, 195107.
(55) Martinez, J. I.; Hansen, H. A.; Rossmeisl, J.; Nørskov, J. K. Formation energies of rutile metal dioxides using density functional theory. *Phys. Rev. B: Condens. Matter Mater. Phys.* **2009**, *79*, 045120.
(56) Seitz, L. C.; Dickens, C. F.; Nishio, K.; Hikita, Y.; Montoya, J.; Doyle, A.; Kirk, C.; Vojvodic, A.; Hwang, H. Y.; Norskov, J. K.; et al. A highly active and stable $IrO_x/SrIrO_3$ catalyst for the oxygen evolution reaction. *Science* **2016**, *353*, 1011−1014.
(57) Viswanathan, V.; Hansen, H. A. Unifying Solution and Surface Electrochemistry: Limitations and opportunities in surface electrocatalysis. *Top. Catal.* **2014**, *57*, 215−221.
(58) Ling, J.; Hutchinson, M.; Antono, E.; Paradiso, S.; Meredig, B. High-Dimensional Materials and Process Optimization Using Data-Driven Experimental Design with Well-Calibrated Uncertainty Estimates. *Integrating Materials and Manufacturing Innovation* **2017**, *6*, 207−217.
(59) Pandey, M.; Jacobsen, K. W. Heats of formation of solids with error estimation: The mBEEF functional with and without fitted reference energies. *Phys. Rev. B: Condens. Matter Mater. Phys.* **2015**, *91*, 235201.
(60) Christensen, R.; Hummelshøj, J. S.; Hansen, H. A.; Vegge, T. Reducing Systematic Errors in Oxide Species with Density Functional Theory Calculations. *J. Phys. Chem. C* **2015**, *119*, 17596−17601.

DOI: 10.1021/acs.jpclett.7b02895
J. Phys. Chem. Lett. 2018, 9, 588−595